

Atomic Solitons in Optical Lattices

S. Pötting^{1,2}, P. Meystre¹ and E. M. Wright¹

¹Optical Sciences Center, University of Arizona
Tucson, AZ 85721, USA

²Max-Planck Institut für Quantenoptik
D-85748 Garching, Germany

I. INTRODUCTION

The experimental demonstration of Bose–Einstein condensation in atomic vapors [1–3] has rapidly lead to spectacular new advances in atom optics. In particular, it has enabled its extension from the linear to the nonlinear regime, very much like the laser lead to the development of nonlinear optics in the 1960s. It is now well established that two-body collisions play for matter waves a role analogous to that of a Kerr nonlinear crystal in optics. In particular, it is known that the nonlinear Schrödinger equation which describes the condensate in the Hartree approximation supports soliton solutions. For the case of repulsive interactions normally encountered in BEC experiments, the simplest solutions are dark solitons, that is, ‘dips’ in the density profile of the condensate. These dark solitons have been recently demonstrated in two experiments [4,5] which appear to be in good agreement with the predictions of the Gross–Pitaevskii equation.

While very interesting from a fundamental physics point-of-view, dark solitons would appear to be of limited potential for applications such as atom interferometry, where it is desirable to achieve the dispersionless transport of a spatially localized ensemble of atoms, rather than a ‘hole’. In that case, bright solitons are much more interesting. However, the problem is that large condensates are necessarily associated with repulsive interactions, for which bright solitons might seem impossible since the nonlinearity cannot compensate for the kinetic energy part (diffraction) in the atomic dynamics. While this is true for atoms in free space, this is however not the case for atoms in suitable potentials, eg. optical lattices. This is because in that case, it is possible to tailor the dispersion relation of the atoms in such a way that their effective mass becomes negative. For such negative masses, a repulsive interaction is precisely what is required to achieve soliton solutions. This result is known from nonlinear optics, where such soliton solutions, called gap solitons, have been predicted and demonstrated [6–9].

The article is organized as follows: In Section II we briefly review the basic formalism for nonlinear atom optics with a focus on Bose condensed systems. This leads to the Gross–Pitaevskii equation, the nonlinear mean-field equation of motion for the atomic condensate. In Section III we introduce the bright and dark soliton solutions of these equations and motivate the concept of gap solitons. In Section IV we then describe a specific model for gap solitons in a spinor Bose–Einstein condensate. We demonstrate how to launch and control these solitons in Section V. Finally, Section VI is a summary and conclusion.

II. NONLINEAR ATOM OPTICS

Early experiments and theories concerning atom optics considered the low-density regime where atom-atom interactions are negligible. However, as the prospect of atomic BEC became more tangible prior to 1995, Lenz *et al.* [10,11] and Zhang *et al.* [12] theoretically explored the high density regime where atom-atom interactions become relevant. In particular, they view the cold atomic collisions as nonlinear mixing processes analogous to those in nonlinear optics, and the new area of nonlinear atom optics was born. These initial theoretical works considered the dipole-dipole interaction between atoms, and derived a mean-field equation for the macroscopic wave function or order parameter for the system of cold atoms analogous to the well-known nonlinear Schrödinger equation from nonlinear optics [13], or the Gross-Pitaevskii equation (GPE) from BEC theory [14,15]. It was shown that these equations admit soliton solutions under suitable conditions [10,12]. The experimental demonstrations of atomic BEC in 1995 in both Rubidium [1] and Sodium [2] ushered in the era of experimental nonlinear atom optics, where the cold atomic collisions are now mediated via the Van der Waals interaction, with experimental demonstrations of atomic four-wave mixing [16], dark atomic solitons [4,5], atomic vortices [17,18], and mode-locking of an atom laser [19].

To set the stage for our discussion, we first briefly review the physics and derivation of the mean-field GPE for an atomic BEC, which underlies nonlinear atom optics. We assume that an ensemble of ultracold atoms of mass m experience a single-particle Hamiltonian of the form

$$H_0 = -\frac{\hbar^2}{2m}\nabla^2 + V(\mathbf{R}) , \quad (1)$$

where the external potential $V(\mathbf{R})$ could be for example an optical dipole potential [20]. In the language of second-quantization this translates to the Hamiltonian operator

$$\hat{\mathcal{H}}_0 = \int d^3r \hat{\Psi}^\dagger(\mathbf{R}) H_0 \hat{\Psi}(\mathbf{R}) , \quad (2)$$

where $\hat{\Psi}^\dagger(\mathbf{R})$ and $\hat{\Psi}(\mathbf{R})$ denote the creation and annihilation operators (in the Schrödinger picture) for an atom with center-of-mass position vector \mathbf{R} . Assuming bosonic atoms, the field operators obey the commutation relation $[\hat{\Psi}(\mathbf{R}), \hat{\Psi}^\dagger(\mathbf{R}')] = \delta(\mathbf{R} - \mathbf{R}')$. Next we add atom-atom interactions by introducing a two-body potential $V(\mathbf{R}, \mathbf{R}')$, which in second-quantization leads to the total Hamiltonian operator $\hat{\mathcal{H}} = \hat{\mathcal{H}}_0 + \hat{\mathcal{V}}$ with

$$\hat{\mathcal{V}} = \frac{1}{2} \int d^3r d^3r' \hat{\Psi}^\dagger(\mathbf{R}) \hat{\Psi}^\dagger(\mathbf{R}') V(\mathbf{R}, \mathbf{R}') \hat{\Psi}(\mathbf{R}') \hat{\Psi}(\mathbf{R}) . \quad (3)$$

For a system of N cold atoms, the many-body state vector may be related to the N -particle Schrödinger wave function using the general relation

$$|\phi_N(t)\rangle = \frac{1}{\sqrt{N!}} \int d^3r_1 \dots d^3r_N \phi_N(\mathbf{R}_1, \dots, \mathbf{R}_N, t) \hat{\Psi}^\dagger(\mathbf{R}_N) \dots \hat{\Psi}^\dagger(\mathbf{R}_1) |0\rangle . \quad (4)$$

Since for a BEC at zero temperature the atoms are predominantly in the same Bose-condensed state, we employ the Hartree approximation in which the N -particle wave function $\phi_N(\mathbf{R}_1, \dots, \mathbf{R}_N, t)$ is written in the form of a product

$$\phi_N(\mathbf{R}_1, \dots, \mathbf{R}_N, t) = \prod_{i=1}^N \vartheta(\mathbf{R}_i, t) , \quad (5)$$

where $\sqrt{N}\vartheta(\mathbf{R}, t) = \langle \phi_{N-1} | \hat{\Psi}(\mathbf{R}) | \phi_N \rangle$ is the effective single-particle, or Hartree, wave function, and is assumed normalized [21]. We note that the Hartree approximation automatically satisfies the symmetry condition for bosons that interchanging any two particle indices produces the same wave function. To obtain an equation of motion for the effective single-particle wave function, we employ Dirac's variational principle [22]

$$\frac{\delta}{\delta \vartheta^*(\mathbf{R}, t)} \left[\langle \phi_N | i\hbar \frac{\partial}{\partial t} - (\hat{\mathcal{H}}_0 + \hat{\mathcal{V}}) | \phi_N \rangle \right] = 0 , \quad (6)$$

which yields the GPE

$$i\hbar \frac{\partial \vartheta}{\partial t} = H_0 \vartheta + (N-1) \int d^3 r' V(\mathbf{R}, \mathbf{R}') |\vartheta(\mathbf{R}', t)|^2 \vartheta(\mathbf{R}, t) . \quad (7)$$

Here the nonlinear term describes the mean-field effect of the $(N-1)$ other atoms on the effective single-particle evolution.

For the particular case of atomic BECs the cold atomic collisions may be treated in the s -wave scattering limit. The effective two-body potential can then be approximated by a contact potential of the form [23,24]

$$V(\mathbf{R}, \mathbf{R}') = U_0 \delta(\mathbf{R} - \mathbf{R}') , \quad (8)$$

where the coefficient $U_0 = 4\pi\hbar^2 a_{sc}/m$, with a_{sc} the s -wave scattering length. The GPE equation (7) for an atomic BEC then becomes

$$i\hbar \frac{\partial \vartheta}{\partial t} = -\frac{\hbar^2}{2m} \nabla^2 \vartheta + V(\mathbf{R}) \vartheta + NU_0 |\vartheta|^2 \vartheta , \quad (9)$$

which applies for large N . This equation forms the basis of the following discussion of atomic solitons. Here we have concentrated on the case of a single atomic species, but the formalism is straightforward to generalize to multi-component or vector condensates [25,26] involving, for example, several different Zeeman sublevels of a given atom.

III. ONE-DIMENSIONAL ATOMIC SOLITONS

A. One-dimensional GPE

In this Section we briefly discuss the one-dimensional (1D) soliton solutions of the GPE (9). In particular, we assume strong transverse confinement of the BEC in the (X, Y) plane such that the transverse mode $u_g(X, Y)$ is the ground state of the potential $V(X, Y)$,

$$E_g u_g = -\frac{\hbar^2}{2m} \left(\frac{\partial^2}{\partial X^2} + \frac{\partial^2}{\partial Y^2} \right) u_g + V(X, Y) u_g . \quad (10)$$

This may be realized, for example, using a red-detuned optical dipole trap around the focus of a Gaussian laser beam centered on the origin [20], thereby giving approximately harmonic transverse confinement. Thus, the BEC becomes essentially one-dimensional with cross-sectional area $A_T = \int dX dY |u_g(X, Y)/u_g(0, 0)|^2$ transverse to the unbound Z -axis. We remark that the quasi-1D nature of the system does not preclude BEC along with the associated GPE description, as discussed by Petrov *et al.* [27]. Setting

$$\sqrt{N}\vartheta(\mathbf{R}, t) = e^{-iE_g t/\hbar} \left(\frac{u_g(X, Y)}{u_g(0, 0)} \right) \varphi(Z, t), \quad (11)$$

so that φ is normalized to the number of atoms N , and projecting onto the ground transverse mode, the reduced 1D GPE becomes (we ignore the variation of the optical potential along the Z -axis for simplicity)

$$i\hbar \frac{\partial \varphi}{\partial t} = -\frac{\hbar^2}{2m} \frac{\partial^2 \varphi}{\partial Z^2} + U|\varphi|^2 \varphi, \quad (12)$$

with $U = U_0 A_T^{-1} \int dX dY |u_g(X, Y)/u_g(0, 0)|^4$.

B. Dark solitons

Soliton solutions are non-spreading solutions of Eq. (12) which preserve their shape under propagation [28]. The kinetic energy term in the GPE tends to spread wavepackets, and the nature of the solitons depends on the sign of the nonlinearity. For the case of repulsive interactions ($a_{sc} > 0$), both the kinetic energy and nonlinearity terms in Eq. (12) tend to broaden localized wavepackets, so we do not expect localized, or bright soliton, solutions for that case. However, dark solitons describing localized density dips in an otherwise constant background can arise and are given by [4,5,29] (with analogous solutions being well known in nonlinear fiber optics e.g. [30])

$$\varphi(Z, t) = n^{1/2} \sqrt{1 - \left(1 - \frac{v^2}{v_0^2}\right) \text{sech}^2 \left(\frac{(Z - vt)}{l_0} \left(1 - \frac{v^2}{v_0^2}\right)^{1/2} \right)} e^{i(\phi(Z, t, v) - \mu t/\hbar)}, \quad (13)$$

where n is the background density away from the dark soliton core, $\mu = n|U|$, $l_0 = \sqrt{\hbar^2/m\mu}$ is the correlation length which determines the width of the soliton core, $v_0 = \sqrt{\mu/m}$ is the Bogoliubov speed of sound, v is the dark soliton velocity, whose magnitude is bounded by v_0 , and the soliton phase ϕ is given by

$$\phi(Z, t, v) = -\arctan \left[\left(\frac{v_0^2}{v^2} - 1 \right)^{1/2} \tanh \left(\frac{(Z - vt)}{l_0} \left(1 - \frac{v^2}{v_0^2}\right)^{1/2} \right) \right]. \quad (14)$$

These solutions show that the dark solitons are characterized by the presence of a phase-step δ across the localized density dip. It can be related to the velocity v and the density n_{bot} at the bottom of the atomic density dip [4,5]. In particular, one finds the relation

$$\cos\left(\frac{\delta}{2}\right) = \frac{v}{v_0} = \frac{n_{bot}}{n}, \quad (15)$$

so that for a stationary soliton $v = 0, n_{bot} = 0$, and there is a $\delta = \pi$ phase-step. Only stationary solitons have a vanishing density at their center, so they are also referred to as ‘black’ solitons, whereas for the $n_{bot} > 0$ case the expression ‘grey’ soliton is used.

Dark matter-wave solitons have recently been observed experimentally in a Na BEC by Denschlag *et al.* [4], and in a cigar-shaped ^{87}Rb condensate by Burger *et al.* [4,5]. In both experiments dark solitons of variable velocity were launched via the phase imprinting of a BEC by a light-shift potential. By applying a pulsed laser to only half of the BEC and choosing the laser intensity and duration to select a desired phase-step δ , the soliton velocity could be selected according to Eq. (15). Fig. 1 shows a schematic of the basic phase-imprinting idea for a cigar-shaped BEC, and Fig. 2 shows the experimental results of Burger *et al.* The motion of the density dip is seen for a phase-step of π and a variety of evolution times. Ideally this value of the phase-step should lead to a stationary dark soliton, but the experiments are carried out in a harmonic trap [31] and dissipative effects were shown to occur that accelerated the solitons [32,33].

C. Bright solitons

For the case of attractive interactions (i.e. $a_{sc} < 0$), the kinetic energy of the BEC can be balanced by the nonlinearity yielding non-spreading wave packets. These solutions correspond to spatially localized bright solitons [29,30]. The one-parameter solution to Eq. (12) then reads

$$\varphi(Z, t) = n^{1/2} \sqrt{2 - \frac{v^2}{v_0^2}} \text{sech} \left[\frac{(Z - vt)}{l_0} \left(2 - \frac{v^2}{v_0^2} \right)^{1/2} \right] e^{i(\phi(Z, t, v) + \mu t / \hbar)}, \quad (16)$$

with v the velocity parameter and μ, l_0 and v_0 as in the dark soliton case. The phase ϕ is given by

$$\phi(Z, t, v) = \frac{(Z - vt)}{l_0} \left(\frac{v}{v_0} \right). \quad (17)$$

Such 1D bright solitons could in principle be realized in cigar shaped BECs with negative scattering lengths, for example, in ^7Li [3] or ^{85}Rb by using Feshbach resonances [34–36] to tune the scattering length. To the best of our knowledge such experiments have not been attempted. In two or more dimensions negative scattering lengths can lead to catastrophic collapse in homogeneous systems for large enough particle numbers. However, in quasi-1D systems with strong transverse confinement the solitons are rendered stable [37].

D. Gap solitons in optical lattices

So far in our discussion dark solitons arise for positive scattering lengths and bright solitons for negative scattering lengths. However, it is possible to extend the range of

options, e.g. bright solitons with a positive scattering length, by considering a 1D BEC in a periodic optical lattice [38,39]. This situation was first discussed by Zhang *et al.* [40] for a scalar or single component condensate, and yields atomic gap solitons. Historically, gap solitons were first considered in nonlinear optics as arising from the combination of optical nonlinearity and a periodic spatial refractive-index distribution [6–9]. As an introduction to our treatment of gap solitons in spinor condensates, we briefly review the physics underlying gap solitons in scalar condensates, referring the reader to the literature for more details [40].

Consider the 1D GPE (12) with an additional periodic potential, or optical lattice, produced by periodic optical fields and applied along the Z-axis, so that

$$i\hbar \frac{\partial \varphi}{\partial t} = -\frac{\hbar^2}{2m} \frac{\partial^2 \varphi}{\partial Z^2} + V_{opt} \cos^2(k_{opt}Z) \varphi + U|\varphi|^2 \varphi. \quad (18)$$

Here V_{opt} determines the strength of the optical lattice, and k_{opt} is the wave vector characteristic of the optical lattice.

Let us first consider the linear eigensolutions of Eq. (18) neglecting the nonlinear term. Introducing the band-index n and the wave vector k within the band, we can write the atomic wave function in terms of the periodic Bloch functions $u_{n,k}(Z)$ according to Bloch's theorem [41]

$$\varphi(Z, t) = \varphi_{n,k}(Z) e^{-iE_{n,k}t/\hbar} = u_{n,k}(Z) e^{i(kZ - E_{n,k}t/\hbar)}.$$

Using this expression in Eq. (18) with $U = 0$, the eigenvalue equation associated with the cosine potential then reads

$$E_{n,k} \varphi_{n,k} = -\frac{\hbar^2}{2m} \frac{d^2 \varphi_{n,k}}{dZ^2} + V_{opt} \cos^2(k_{opt}Z) \varphi_{n,k}, \quad (19)$$

the eigenvectors and eigenvalues of which are well known [42]. For our discussion the important fact is the occurrence of an atomic band structure given by the dispersion relation $E_{n,k} = \hbar \omega_{n,k}$. Consider an atomic wavepacket for a given band-index n and a narrow spread of wave vectors Δk around a central value k_0 that is slowly varying on the scale of the periodicity. Then we can write the atomic wave function as a product of the slowly varying envelope $\chi(Z, t)$ with the fast oscillating Bloch part

$$\varphi(Z, t) = \chi(Z, t) \varphi_{n,k_0} e^{-iE_{n,k_0}t/\hbar}. \quad (20)$$

In this approximation the group velocity v_g and effective mass m_{eff} for the wavepacket will be

$$v_g = \frac{1}{\hbar} \frac{\partial E_{n,k}}{\partial k} \Big|_{k_0}, \quad \frac{1}{m_{eff}} = \frac{1}{\hbar^2} \frac{\partial^2 E_{n,k}}{\partial k^2} \Big|_{k_0}, \quad (21)$$

in terms of which the approximate dynamics of the slowly varying envelope $\chi(Z, t)$ may be described by

$$i\hbar \left(\frac{\partial}{\partial t} + v_g \frac{\partial}{\partial Z} \right) \chi = -\frac{\hbar^2}{2m_{eff}} \frac{\partial^2 \chi}{\partial Z^2} + U|\chi|^2 \chi, \quad (22)$$

where we have re-introduced the nonlinearity.

We take for illustration the case $k_0 = 0$, that is zone center, so that $v_g = 0$. Then Eq. (22) becomes identical with Eq. (12), so that they have the same bright and dark soliton solutions but with $m \rightarrow m_{eff}$. The key idea is that the effective mass m_{eff} can assume both positive and negative signs by a suitable choice of the band index n and k_0 , whereas for the spatially homogeneous case the atomic mass m is always positive. So now, for example, bright solitons can arise for a positive scattering length if the effective mass is negative, the general condition for bright solitons being $m_{eff}U < 0$, and conversely for dark solitons $m_{eff}U > 0$. We remark that the applied optical lattice can modify the effective mass along the Z -axis, but the effective mass along the transverse dimensions is still m . This leaves open the question of higher-dimensional gap solitons, a point that we do not further address here [43].

The solitons formed in optical lattices are referred to as gap solitons [7–9]. This name derives from the fact that the soliton energies actually lie in the energy gaps of the atomic band structure [6]. The significance of gap solitons in the context of atomic BEC is that they provide a means to realize bright solitons, that is, spatially localized atomic packets, *even for positive scattering lengths*. This may have important applications, e.g. for the coherent transport of atoms. In the following section we further develop the theory of atomic gap solitons in spinor condensates to quantify some of their most important properties.

IV. ATOMIC GAP SOLITONS

We now consider a system of two condensates in different Zeeman sublevels coupled by a spatially periodic two-photon interaction. This spatially modulated coupling again leads to an atomic band structure for the spinor condensate, and hence by our general arguments of the previous section, to gap solitons. The advantage of multicomponent condensates is that magnetic fields can now be used to phase-imprint the two Zeeman components differently, and hence to manipulate and control the gap solitons to a high degree. We demonstrate this flexibility in Section V by simulating an atomic interferometer based on gap solitons.

A. The physical model for a spinor condensate

The two-component Bose–Einstein condensate interacts with two counterpropagating, focused Gaussian laser beams of equal frequencies ω_l but opposite circular polarizations. The optical dipole potential associated with the applied laser beams is assumed to provide tight transverse confinement for the BEC in the (X, Y) plane, thereby forming a cigar-shaped condensate of transverse cross-sectional area A_T . As in Section III, we confine our discussion to the one-dimensional dynamics of the BEC along the Z -axis for simplicity.

In addition to supplying a transverse optical potential, the laser beams can drive two-photon transitions between different Zeeman sublevels of the atomic ground state. For illustrative purposes we consider the case of Sodium and the two-photon coupling of the Zeeman sublevels $|-1\rangle = |F_g = 1, M_g = -1\rangle$ and $|1\rangle = |F_g = 1, M_g = 1\rangle$. For example, starting in the $|-1\rangle$ state this process involves the absorption of a σ_+ photon from the right propagating laser beam followed by emission of a σ_- photon into the left propagating laser beam. We must of course assume that the excited states involved in the atom-field

interaction are far-detuned from the applied laser frequency, a necessary requirement to avoid the detrimental effects of spontaneous emission.

By restricting our attention to the coupled states $|\pm 1\rangle$ the effective single-particle Hamiltonian for our model system can be written as [44,45]

$$H_{\text{eff}} = \frac{P_Z^2}{2m} + g\hbar\delta' \left[|1\rangle \langle -1| e^{2iK_l Z} + |-1\rangle \langle 1| e^{-2iK_l Z} \right], \quad (23)$$

where we have omitted constant light-shift terms. Here P_Z is the atomic center-of-mass momentum operator along Z , $K_l = \omega_l/c$ is the magnitude of the field wave vector along Z , g is a coupling constant between the ground and excited states characteristic of the atom and transition involved, $\delta' = \mathcal{D}^2 \mathcal{E}^2 / \hbar^2 \delta$, with the detuning $\delta = \omega_l - \omega_a$, \mathcal{E} is the laser field amplitude, and \mathcal{D} is the reduced electric dipole moment for the $3S_{1/2}$ - $3P_{3/2}$ transition.

The second term of the effective Hamiltonian (23) describes the effective coupling of the two Zeeman sublevels via the applied laser fields. The exponential terms $\exp(\pm 2iK_l Z)$ arise from the fact that the two-photon transitions involve the absorption of a photon from one light field and reemission into the other. Introducing a spinor macroscopic condensate wave function $\varphi(Z, t) = [\varphi_1(Z, t), \varphi_{-1}(Z, t)]^T$ normalized to the number of atoms N , and including the many-body effects via a mean-field nonlinearity, we obtain the coupled GPE equations

$$i\hbar \frac{\partial \varphi}{\partial t} = H_{\text{eff}} \varphi + U |\varphi|^2 \varphi, \quad (24)$$

where $U = 4\pi\hbar^2 a_{sc}/m$ as in Section II and III, $|\varphi|^2 = |\varphi_1|^2 + |\varphi_{-1}|^2$, and we have assumed that the magnitude of the self- and cross-nonlinearities are equal for simplicity.

It is convenient to re-express Eq. (24) in dimensionless form by introducing the scaled variables $t = \tau t_c$, $Z = z l_c$ and $\varphi_j = \psi_j \sqrt{\rho_c}$ where

$$t_c = \frac{1}{g\delta'}, \quad l_c = \frac{t_c \hbar K_l}{m}, \quad \rho_c = \left| \frac{g\hbar\delta'}{U} \right|. \quad (25)$$

Equations (24) then become

$$\begin{aligned} i \frac{\partial}{\partial \tau} \begin{pmatrix} \psi_1 \\ \psi_{-1} \end{pmatrix} &= \begin{pmatrix} -M \nabla^2 & e^{2ik_l z} \\ e^{-2ik_l z} & -M \nabla^2 \end{pmatrix} \begin{pmatrix} \psi_1 \\ \psi_{-1} \end{pmatrix} \\ &+ \text{sgn}(g\delta'/U) |\psi|^2 \begin{pmatrix} \psi_1 \\ \psi_{-1} \end{pmatrix}, \end{aligned} \quad (26)$$

where $M = g\delta' m / 2\hbar K_l^2$ is a mass-related parameter such that $k_l = K_l l_c = 1/2M$. For a discussion of characteristic values for the case of a Sodium condensate we refer the reader to Ref. [46].

B. Soliton solutions

The spatially modulated coupling between the optical fields and the condensate induces a single-particle band structure with regions of negative effective mass. As mentioned before, this leads to the possibility of bright atomic solitons even for repulsive interactions [44].

Approximate analytic expressions for these solitons can be obtained by expressing the spinor condensate components as

$$\psi_{\pm 1}(z, \tau) = e^{\pm i k_l z} e^{-i \tau / 4M} \phi_{\pm 1}(z, \tau) , \quad (27)$$

where the field envelopes $\phi_{\pm 1}$ are assumed to be slowly varying in space compared to $1/k_l$. Neglecting the second-order spatial derivatives yields the coupled partial differential equations

$$i \left(\frac{\partial}{\partial \tau} \pm \frac{\partial}{\partial z} \right) \begin{pmatrix} \phi_1 \\ \phi_{-1} \end{pmatrix} = \begin{pmatrix} 0 & 1 \\ 1 & 0 \end{pmatrix} \begin{pmatrix} \phi_1 \\ \phi_{-1} \end{pmatrix} \pm (|\phi_1|^2 + |\phi_{-1}|^2) \begin{pmatrix} \phi_1 \\ \phi_{-1} \end{pmatrix} , \quad (28)$$

where the choice $\pm 1 = \text{sgn}(g\delta'/U)$. For a red-detuned laser and our choice of g this becomes $\pm 1 = \text{sgn}(U)$. Neglecting the nonlinearity one finds a linear dispersion curve as sketched in Fig. 3. In this particular case it is the linear coupling induced by the laser field that creates the avoided crossing at $k = 0$ and the negative effective mass. Aceves and Wabnitz [47] have shown that the full equations (28) have the explicit two-parameter gap soliton solutions (see also Ref. [8])

$$\begin{aligned} \phi_1 &= \pm \frac{\sin(\eta)}{\beta \gamma \sqrt{2}} \left(-\frac{e^{2\theta} + e^{\mp i \eta}}{e^{2\theta} + e^{\pm i \eta}} \right)^v \text{sech} \left(\theta \mp \frac{i \eta}{2} \right) e^{\pm i \sigma} , \\ \phi_{-1} &= -\frac{\beta \sin(\eta)}{\gamma \sqrt{2}} \left(-\frac{e^{2\theta} + e^{\mp i \eta}}{e^{2\theta} + e^{\pm i \eta}} \right)^v \text{sech} \left(\theta \pm \frac{i \eta}{2} \right) e^{\pm i \sigma} . \end{aligned} \quad (29)$$

Here $-1 < v < 1$ is a parameter which controls the soliton velocity, $0 < \eta < \pi$ is a shape parameter, and

$$\beta = \left(\frac{1-v}{1+v} \right)^{\frac{1}{4}} , \quad \gamma = \frac{1}{\sqrt{1-v^2}} , \quad (30)$$

$$\theta = -\gamma \sin(\eta)(z - v\tau) , \quad \sigma = -\gamma \cos(\eta)(vz - \tau) . \quad (31)$$

Since we are interested in creating bright solitons in the presence of repulsive interactions we restrict ourselves to $\text{sgn}(U) = +1$, corresponding to the choice of the upper sign in the analytic solutions. The characteristic length scale associated with the solitons is l_c , so that the approximate solitons (29) are valid for $K_l l_c = 1/2M \gg 1$.

C. Soliton properties

From the dependence of the hyperbolic-secant on $\theta = -\gamma \sin(\eta)(z - v\tau)$ in Eqs. (29), we identify the gap soliton parameter $v = V_g/V_R$ as the group velocity V_g of the soliton in units of the recoil velocity $V_R = l_c/t_c = \hbar K_l/m$. Since $-1 < v < 1$, the magnitude of the group velocity is bounded by the recoil velocity. From Eqs. (29), one can extract further

important soliton properties, such as the number N_s of atoms in the soliton and the soliton width $W_s = w_s l_c$. Specifically, the number of atoms in a particular gap soliton is given by

$$N_s = A_T \int dZ [|\varphi_1(Z, t)|^2 + |\varphi_{-1}(Z, t)|^2] , \quad (32)$$

where A_T is the effective transverse area.

We can gain further insight into the analytical structure of the gap solitons by taking the extreme limit $\eta \ll 1$ of Eqs. (29). Using the definitions (27) and returning to dimensional units, we have then

$$\begin{aligned} \varphi_1(Z, 0) &= \frac{\eta}{\beta\gamma} \sqrt{\frac{\rho_c}{2}} \text{sech}(Z/W_0) (-1)^v e^{i(K+K_l)Z} , \\ \varphi_{-1}(Z, 0) &= \frac{\beta\eta}{\gamma} \sqrt{\frac{\rho_c}{2}} \text{sech}(Z/W_0) (-1)^v e^{i[(K-K_l)Z+\pi]} , \end{aligned} \quad (33)$$

where

$$W_s = 3.44W_0 = 3.44 \left(\frac{l_c \sqrt{1-v^2}}{\eta} \right) , \quad K = -\frac{\gamma v}{l_c} . \quad (34)$$

Here $W_s = 3.44W_0$ is the soliton width, the factor 3.44 being the numerical conversion from the width of the hyperbolic secant to the $1/e^2$ width of the distribution, and $K = k/l_c$ a velocity-dependent wave vector shift. Obviously the width decreases with increasing η and v . The soliton atom number obtained by combining Eqs. (32) and (33),

$$N_s = 2(A_T l_c \rho_c) \eta \cdot (1 - v^2) , \quad (35)$$

predicts that increasing the shape parameter η increases the atom number, and faster solitons have lower atom numbers.

An essential point to keep in mind is that the gap solitons are coherent superpositions of the two Zeeman sublevels. The approximate solutions (33) contain important information on the phase and amplitude relations that need to be created between them to successfully excite and manipulate gap solitons. In particular, they show that there is always a spatially homogeneous π phase difference between the two states. In addition, the two components have the spatial wave vectors

$$K_{\pm 1} = K \pm K_l , \quad (36)$$

with $K = -\gamma v/l_c$.

Finally, it follows from dividing the amplitudes of the two components that

$$\left| \frac{\varphi_1(Z, t)}{\varphi_{-1}(Z, t)} \right|^2 = \frac{1}{\beta^4} = \left(\frac{1+v}{1-v} \right) , \quad (37)$$

which shows that their relative occupation depends on the soliton velocity parameter v . For $v = 0$ the sublevels are equally populated, but as $v \rightarrow 1$ the $|1\rangle$ sublevel has a larger population, and vice versa for $v \rightarrow -1$.

The characteristic time scale for the evolution of the gap solitons can be determined from the plane-wave exponential factors in Eqs. (29). Converting back to dimensional form the soliton period t_s is defined as the time to accumulate a 2π phase, or in the limit $\eta \rightarrow 0$

$$t_s = 2\pi t_c \sqrt{1 - v^2}. \quad (38)$$

Physically, t_s corresponds to the internal time scale for the gap soliton. In order to observe a soliton-like behavior, it is therefore necessary to investigate the atomic propagation over several periods.

We conclude this section by noting that Aceves and Wabnitz [47] have shown that the gap soliton solutions (29) are stable solutions of Eqs. (28) in that they remain intact during propagation, even when perturbed away from the exact solutions. However, one should remember that Eq. (28) is only an approximation to the exact system of equations (26), so that in general the gap solitons are solitary wave solutions only. As such, they are not guaranteed to be absolutely stable.

V. MAGNETO-OPTICAL CONTROL

Summarizing the main results of the preceding section, we have seen that gap solitons require the right population and density distribution in each Zeeman sublevel, a certain phase difference between these sublevels, and appropriate plane-wave factors $e^{iK_{\pm 1}Z}$. Based on these properties, we now show that a magneto-optical scheme involving a combination of pulsed coherent optical coupling and of phase-imprinting using spatially inhomogeneous magnetic fields turn out to be an adequate and convenient tool to manipulate these solitons.

A. Manipulation Tools

The shapes of the Hartree wave functions corresponding to the two Zeeman sublevels are hyperbolic-secant, which we approximate by a Gaussian in the following. They could for example be initialized in an optical dipole trap [20]. Manipulating the gap solitons reduces therefore to the problem of controlling the populations and phases throughout the spinor condensate. The coherent optical coupling can be achieved e.g. by a laser pulse of frequency ω_l propagating perpendicularly to the Z -axis and with linear polarization perpendicular to that axis. For sufficiently short pulses, one can neglect changes in the center-of-mass motion of the atoms during its duration, leading to a very simple description. We assume for simplicity a plane-wave rectangular pulse of duration t_p and of spatial extent large compared to the soliton. The Hamiltonian describing the coupling between this pulse and the condensate is then the same as in Eq. (23), but without the linear momentum exchange terms $\exp(\pm 2iK_l Z)$ and the kinetic energy term, and with $\delta' \rightarrow \delta'_p$. The state of the system after the pulse is then easily found to be

$$\begin{aligned} \begin{pmatrix} \varphi_1(t_p) \\ \varphi_{-1}(t_p) \end{pmatrix} &= \begin{pmatrix} \cos \chi & i \sin \chi \\ -i \sin \chi & \cos \chi \end{pmatrix} \begin{pmatrix} \varphi_1(0) \\ \varphi_{-1}(0) \end{pmatrix} \\ &\equiv M_L(\chi) \begin{pmatrix} \varphi_1(0) \\ \varphi_{-1}(0) \end{pmatrix}. \end{aligned} \quad (39)$$

where $\chi = g\delta'_p t_p$ is the excitation pulse area and the operator M_L can be used to control the population transfer by an appropriate choice of χ .

The required phase relationship between the two states can be achieved via Zeeman splitting. Considering for concreteness a spatially inhomogeneous rectangular magnetic field pulse of duration t_B we have, neglecting again all other effects,

$$i\hbar \frac{\partial}{\partial t} \varphi_{\pm 1}(Z, t) = \pm \mu_B g_F (B_0 + B'Z) \varphi_{\pm 1}(Z, t);, \quad (40)$$

where g_F is the Landé g-factor of the hyperfine ground state, μ_B is the Bohr magneton, B_0 the spatially homogeneous component of the magnetic field, and B' its gradient, the direction of the magnetic field being along the Z -axis. The application of this field results in the state

$$\begin{aligned} \begin{pmatrix} \varphi_1(t_B) \\ \varphi_{-1}(t_B) \end{pmatrix} &= \begin{pmatrix} e^{i(\vartheta + K_B Z)} & 0 \\ 0 & e^{-i(\vartheta + K_B Z)} \end{pmatrix} \begin{pmatrix} \varphi_1(0) \\ \varphi_{-1}(0) \end{pmatrix} \\ &\equiv M_B(\vartheta, K_B) \begin{pmatrix} \varphi_1(0) \\ \varphi_{-1}(0) \end{pmatrix}, \end{aligned} \quad (41)$$

where $\vartheta = -(\mu_B g_F / \hbar) B_0 t_B$ and $K_B = -(\mu_B g_F / \hbar) B' t_B$ are the imprinted phase shift and phase gradient (or wave vector), respectively. That is, the application of the magnetic pulse results in a phase difference of 2ϑ between the two Zeeman sublevels, and in addition it imparts them wave vectors $\pm K_B$.

B. Excitation and Application

To illustrate how stationary and moving solitons can be excited using this scheme, we start from a scalar condensate in the $|-1\rangle$ state, $\varphi(Z, 0) = [0, \varphi_0(z)]^T$, with spatial mode

$$\varphi_0(Z) = \frac{N_s}{\sqrt{A_T}} \left(\frac{2}{\pi W_s^2} \right)^{1/4} e^{-Z^2/W_s^2}, \quad (42)$$

with W_s and N_s the width and atom number of the gap soliton desired. This Gaussian is chosen to approximate the hyperbolic-secant structure of the analytic gap soliton solution in Eq. (33). For a stationary solution we need to prepare the Zeeman sublevels with equal populations and with a π phase difference. We further need to impose wave vectors which are equal in magnitude but opposite in sign, $K_{\pm 1} = \pm K_l$. This can be achieved by applying a laser pulse of area $\chi = \pi/4$, followed by a magnetic pulse with $\vartheta = \pi/4$ and $K_B = K_l$. The state then transforms as ($t = t_p + t_B$)

$$\begin{aligned} \varphi(Z, t) &= M_B(\pi/4, K_l) M_L(\pi/4) \varphi(Z, 0) \\ &= \frac{e^{\frac{3i\pi}{4}}}{\sqrt{2}} \begin{pmatrix} e^{iK_l Z} \\ e^{-i\pi} e^{-iK_l Z} \end{pmatrix} \varphi_0(Z). \end{aligned} \quad (43)$$

Figure 4 shows the resulting stable evolution of the total density $|\varphi(Z, t)|^2$. As a result of the Gaussian approximation to the exact solution there are some slow oscillations imposed on

the motion, but the solution remains centered at $Z = 0$ and stationary over a time $t = 200$ ms, much longer than the soliton period for the chosen values. We note that although Section V A treated the pulsed excitations in an impulsive manner to intuitively understand their action, our simulations do not make this approximation. The numerics confirm the accuracy of the impulsive approximation for the parameters at hand; a consequence of the fact that we consider pulse durations significantly shorter than the soliton period (38).

The excitation of a moving soliton is slightly more complicated since the velocity dependent wave vector $K = -\gamma v/l_c$ in Eq. (33) is no longer zero and the two components have different populations, see Eq. (37). However, our simulations show that the proposed scheme performs well on this task, as well as on splitting solitons and reversing their directions [46].

Solitons present some advantages for atom interferometry in that they are many-atom wavepackets which are immune to the effects of spreading, hence allowing longer path lengths, and also increased signal-to-noise for large atom numbers. Typically many-body effects limit the utility of high-density wavepackets due to spatially varying mean-field phase shifts, but solitons have the cardinal virtue that they have fixed spatial phase variations. Thus they may provide a key to making maximal use of high density sources for atom interferometry. Indeed, due to these very properties they have long been advocated for all-optical switching applications.

VI. SUMMARY

In this paper, we have reviewed important aspects of the matter-wave solitons that can be launched in weakly interacting Bose–Einstein condensates. So far, only dark solitons have been demonstrated experimentally, but the rapid progress in the optical manipulation and control of condensates is expected to lead to the demonstration of bright gap solitons.

As an illustration of the potential use of these objects, we consider a soliton-based nonlinear atomic Mach–Zehnder interferometer. Our specific demonstration involves an initial scalar condensate that is split into two oppositely moving solitons along Z , see Fig. 5 for $t < 60$ ms. At $t = 60$ ms laser and magnetic pulses are applied which act to reverse the direction of the two solitons. This process causes some loss of atoms in both solitons, as before. The two reversed soliton components come together again at $t = 120$ ms. Since the colliding solitons are predominantly in opposite orthogonal Zeeman sublevels, the interference pattern appearing during the collision is due to the contamination of each soliton by the other state. Fig. 6 shows the interference at the soliton collision in the total density (solid line) and also the individual Zeeman sublevels, with a fringe contrast of around 30%. These results demonstrate the potential use of gap solitons for realizing nonlinear atom interferometers with high brightness sources.

ACKNOWLEDGMENTS

The authors would like to thank the Hannover group for providing Figs. 1 and 2 as well as K. M. Hilligsoe for pointing out a mistake in (21). This work is supported in part by Office of Naval Research Contract Nos. 14-91-J1205 and N00014-99-1-0806, the National Science

Foundation Grant PHY98-01099, the Army Research Office and the Joint Services Optics Program.

REFERENCES

- [1] M. H. Anderson, J. R. Ensher, M. R. Matthews, C. E. Wieman, and E. A. Cornell, *Science* **269**, 198 (1995).
- [2] K. B. Davis, M.-O. Mewes, M. R. Andrews, N. J. van Druten, D. S. Durfee, D. M. Kurn, and W. Ketterle, *Phys. Rev. Lett.* **75**, 3969 (1995).
- [3] C. C. Bradley, C. A. Sackett, J. J. Tollett, and R. G. Hulet, *Phys. Rev. Lett.* **75**, 1687 (1995).
- [4] J. Denschlag, J. E. Simsarian, D. L. Feder, C. W. Clark, L. A. Collins, J. Cubizolles, L. Deng, E. W. Hagley, K. Helmerson, W. P. Reinhardt, S. L. Rolston, B. I. Schneider, and W. D. Phillips, *Science* **287**, 97 (2000).
- [5] S. Burger, K. Bongs, S. Dettmer, W. Ertmer, K. Sengstock, A. Sanpera, G. V. Shlyapnikov, and M. Lewenstein, *Phys. Rev. Lett.* **83**, 5198 (1999).
- [6] W. Chen and D. L. Mills, *Phys. Rev. Lett.* **58**, 160 (1987).
- [7] D. N. Christodoulides and R. I. Joseph, *Phys. Rev. Lett.* **62**, 1746 (1989).
- [8] C. M. de Sterke and J. E. Sipe, *Gap Solitons*. In *Progress in Optics*, Vol. XXXIII, edited by E. Wolf (Elsevier, Amsterdam, 1994), pp. 203-260.
- [9] B. J. Eggleton, R. E. Slusher, C. M. de Sterke, P. A. Krug, and J. E. Sipe, *Phys. Rev. Lett.* **76**, 1627 (1996).
- [10] G. Lenz, P. Meystre, and E. M. Wright, *Phys. Rev. Lett.* **71**, 3271 (1993).
- [11] G. Lenz, P. Meystre, and E. M. Wright, *Phys. Rev. A* **50**, 1681 (1994).
- [12] W. Zhang, D. F. Walls, and B. C. Sanders, *Phys. Rev. Lett.* **72**, 60 (1994).
- [13] A. C. Newell and J. V. Moloney, *Nonlinear Optics* (Addison-Wesley, Redwood City, 1992).
- [14] L. P. Pitaevskii, *Sov. Phys. JETP* **13**, 451 (1961).
- [15] E. P. Gross, *J. Math. Phys.* **4**, 195 (1963).
- [16] L. Deng, E. W. Hagley, J. Wen, M. Trippenbach, Y. Band, P. S. Julienne, J. E. Simsarian, K. Helmerson, S. L. Rolston, and W. D. Phillips, *Nature* **398**, 218 (1999).
- [17] M. R. Matthews, B. P. Anderson, P. C. Haljan, D. S. Hall, C. E. Wieman, and E. A. Cornell, *Phys. Rev. Lett.* **83**, 2498 (1999).
- [18] K. W. Madison, F. Chevy, W. Wohlleben, and J. Dalibard, *Phys. Rev. Lett.* **84**, 806 (2000).
- [19] B. P. Anderson and M. A. Kasevich, *Nature* **282**, 1686 (1998).
- [20] D. M. Stamper-Kurn, M. R. Andrews, A. P. Chikkatur, S. Inouye, H.-J. Miesner, J. Stenger, and W. Ketterle, *Phys. Rev. Lett.* **80**, 2027 (1998).
- [21] E. M. Lifshitz and L. P. Pitaevskii, *Statistical Physics: Part 2*, (Pergamon Press, Oxford, 1980).
- [22] P. A. M. Dirac, *Proc. Camb. Phil.* **26**, 376 (1930).
- [23] E. M. Lifshitz and L. P. Pitaevskii, *Quantum Mechanics: Part 3*, (Pergamon Press, Oxford, 1991).
- [24] K. Huang, *Statistical Mechanics*, (Wiley, New York, 1987).
- [25] E. V. Goldstein and P. Meystre, *Phys. Rev. A* **55**, 2935 (1997).
- [26] H. Pu and N. P. Bigelow, *Phys. Rev. Lett.* **80**, 1130 (1998).
- [27] D. S. Petrov, G. V. Shlyapnikov, and J. T. M. Walraven, *Regimes of quantum degeneracy in trapped 1D gases*, cond-mat/0006339.
- [28] A. C. Scott, F. Y. F. Chu, and D. W. McLaughlin, *Proc. IEEE* **61**, 1443 (1973).

- [29] W. P. Reinhardt and C. W. Clark, J. Phys. B **30**, L785 (1997).
- [30] G. P. Agrawal, *Nonlinear Fiber Optics*, (Academic Press, San Diego, 1995).
- [31] R. Dum, J. I. Cirac, M. Lewenstein, and P. Zoller, Phys. Rev. Lett. **80**, 2972 (1998).
- [32] P. O. Fedichev, A. E. Muryshev, and G. V. Shlyapnikov, Phys. Rev. A **60**, 3220 (1999).
- [33] T. Busch and J. R. Anglin, Phys. Rev. Lett. **84**, 2298 (2000).
- [34] S. L. Cornish, N. R. Claussen, J. L. Roberts, E. A. Cornell, and C. E. Wieman, Phys. Rev. Lett. **85**, 1795 (2000).
- [35] J. L. Roberts, N. R. Claussen, J. P. Burke, Jr., C. H. Greene, E. A. Cornell, and C. E. Wieman, Phys. Rev. Lett. **81**, 5109 (1998).
- [36] S. Inouye, M. R. Andrews, J. Stenger, H.-J. Miesner, D. M. Stamper-Kurn, and W. Ketterle, Nature **392**, 151 (1998).
- [37] Y. S. Kivshar and T. J. Alexander, *Trapped Bose–Einstein Condensates: Role of Dimensionality*, cond-mat/9905048.
- [38] K. Berg-Sørensen and K. Mølmer, Phys. Rev. A **58**, 1480 (1998).
- [39] D.-I. Choi and Q. Niu, Phys. Rev. Lett. **82**, 2022 (1999).
- [40] M. J. Steel and W. Zhang, *Bloch function description of a Bose–Einstein condensate in a finite optical lattice*, cond-mat/9810284.
- [41] C. Kittel, *Introduction to Solid State Physics*, (Wiley, New York, 1986).
- [42] M. Abramowitz and I. A. Stegun, *Handbook of Mathematical Functions*, (Dover, New York, 1970).
- [43] N. Aközbek and S. John, Phys. Rev. E **57**, 2287 (1998).
- [44] O. Zobay, S. Pötting, P. Meystre, and E. M. Wright, Phys. Rev. A **59**, 643 (1999).
- [45] C. Cohen-Tannoudji, *Atomic Motion in Laser Light*. In *Fundamental Systems in Quantum Optics*, edited by J. Dalibard, J. M. Raimond, and J. Zinn-Justin (North-Holland, Amsterdam, 1992), pp. 1-164.
- [46] S. Pötting, O. Zobay, P. Meystre, and E. M. Wright, J. Mod. Opt. (*to be published*).
- [47] A. B. Aceves and S. Wabnitz, Phys. Lett. A **141**, 37 (1989).

FIGURES

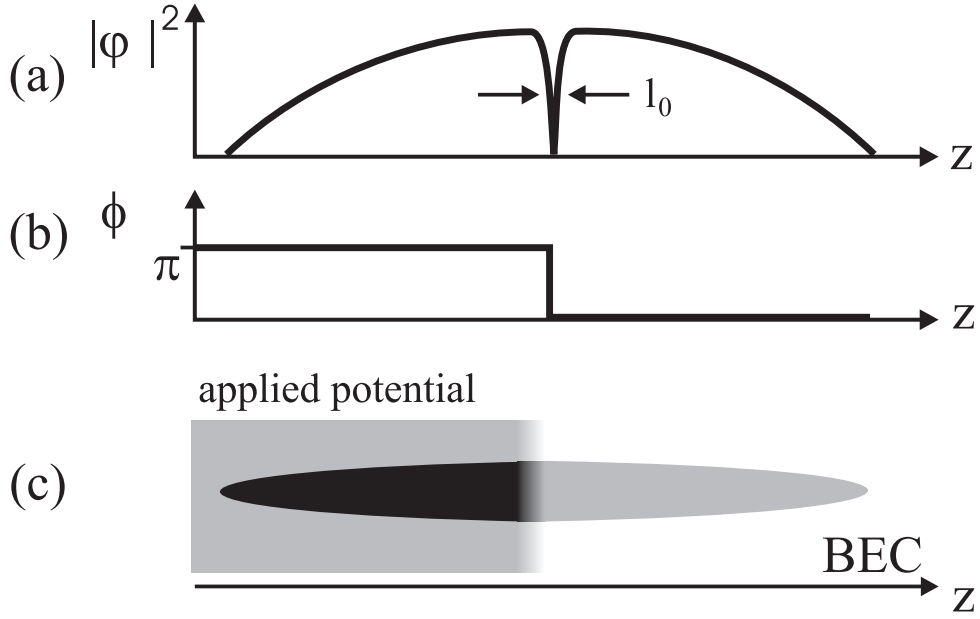


FIG. 1. Density distribution **(a)** and spatial phase **(b)** of a stationary dark soliton with $\delta = \pi$. The dip in the density has a width $\sim l_0$. The scheme for the generation of dark solitons by phase imprinting is shown in **(c)**

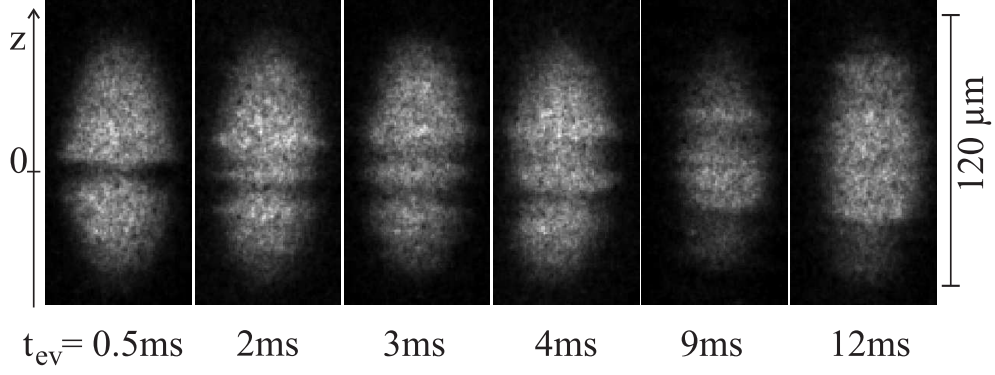


FIG. 2. Absorption images of BECs with dark soliton structures propagating along the long condensate axis for different evolution times t_{ev}

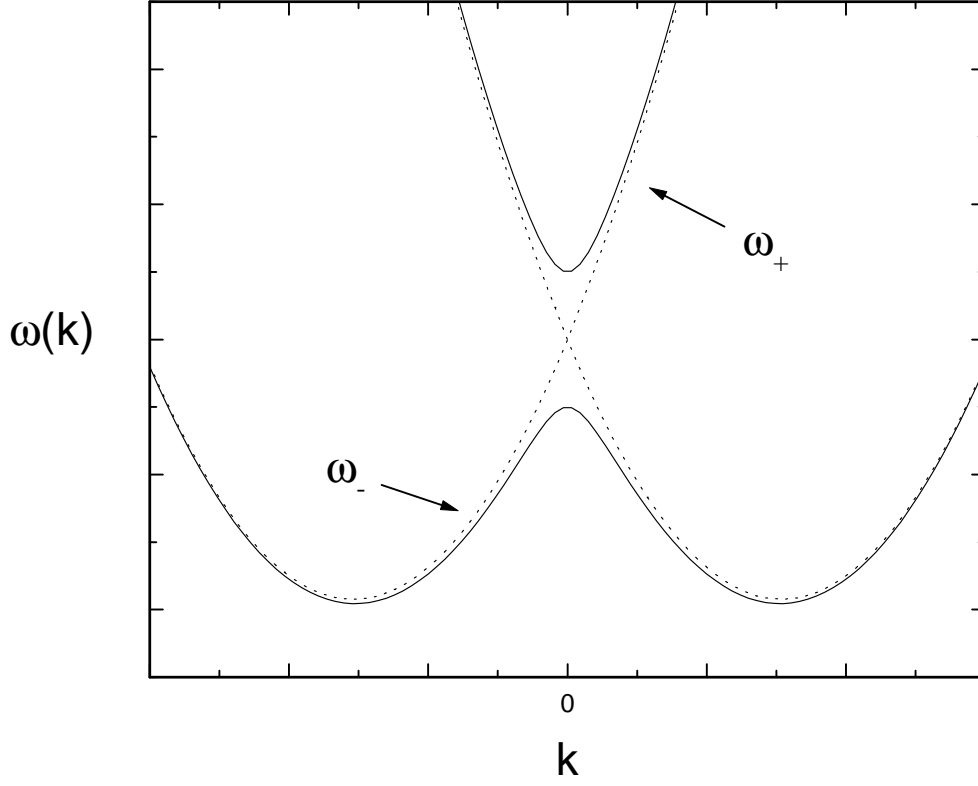


FIG. 3. Linear dispersion curve (arbitrary units): Shown are the two branches of the dispersion relation exhibiting an avoided crossing at $k = 0$ (*solid line*). The negative curvature in the lower branch around $k = 0$ defines a negative effective mass that enables gap soliton solutions. The free dispersion when no linear coupling is present corresponds to two displaced parabolas (*dashed line*)

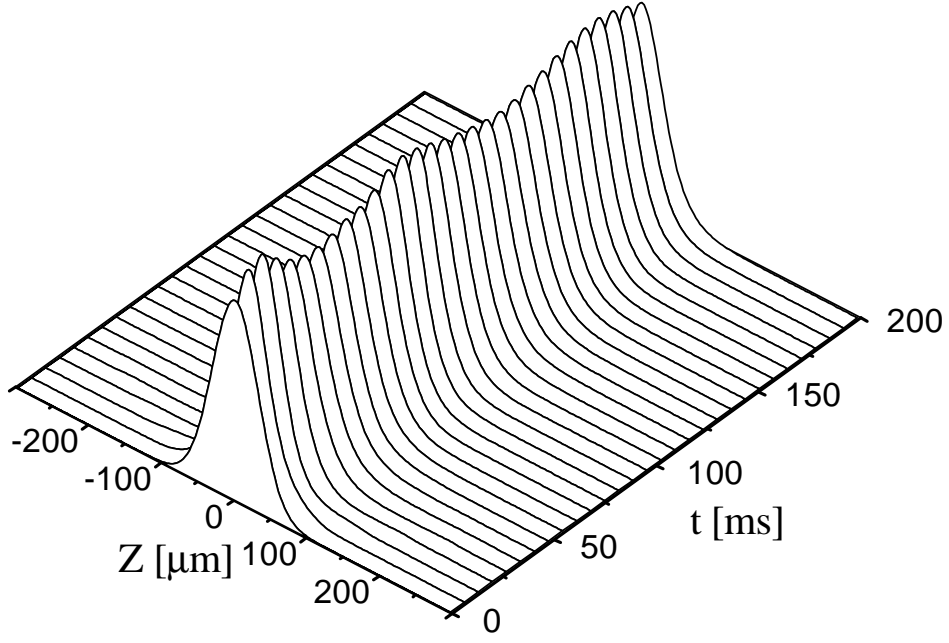


FIG. 4. The propagation of the total density of a stationary soliton ($v = 0$) over around 50 soliton periods. Peak density oscillations are due to imperfect initial conditions

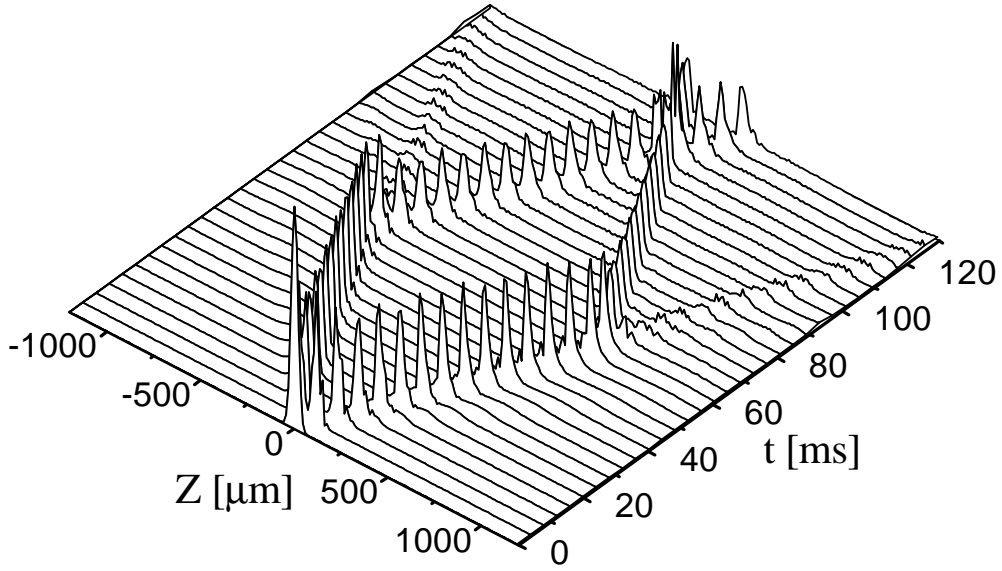


FIG. 5. Demonstration of an atomic Mach–Zehnder interferometer: The initial condensate is split into two counterpropagating solitons, then their direction is reversed and they collide (shown is the total density)

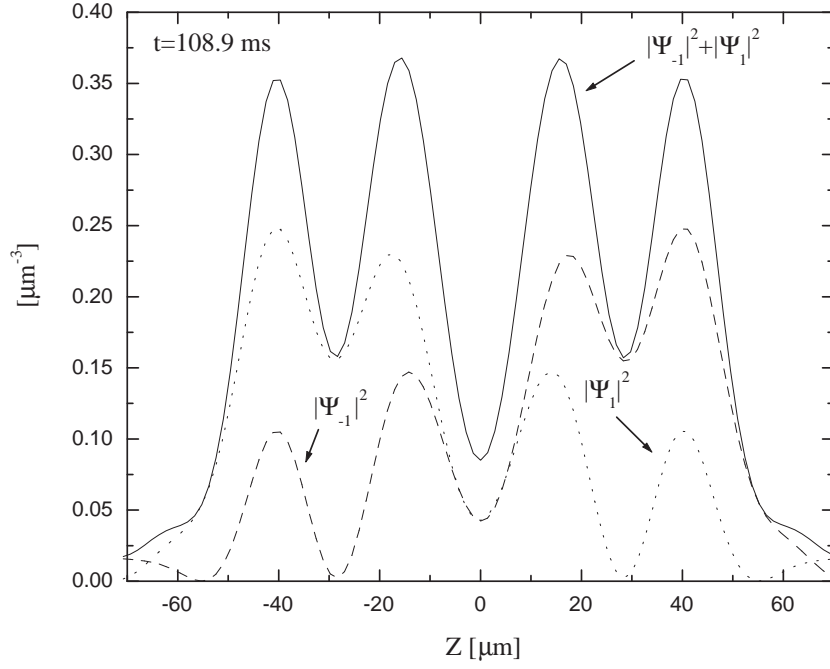


FIG. 6. Interference pattern when two solitons collide in the Mach-Zehnder configuration: The total density (*solid line*) is symmetric, whereas the interference pattern of each of the two orthogonal Zeeman states (*dotted* and *dashed line*) is asymmetric due to the shape of the colliding wavepackets. The contrast in the total density pattern is around 30%